Stroke and migraine: Translational studies into a complex relationship
Mulder, I.A.

Cover Page

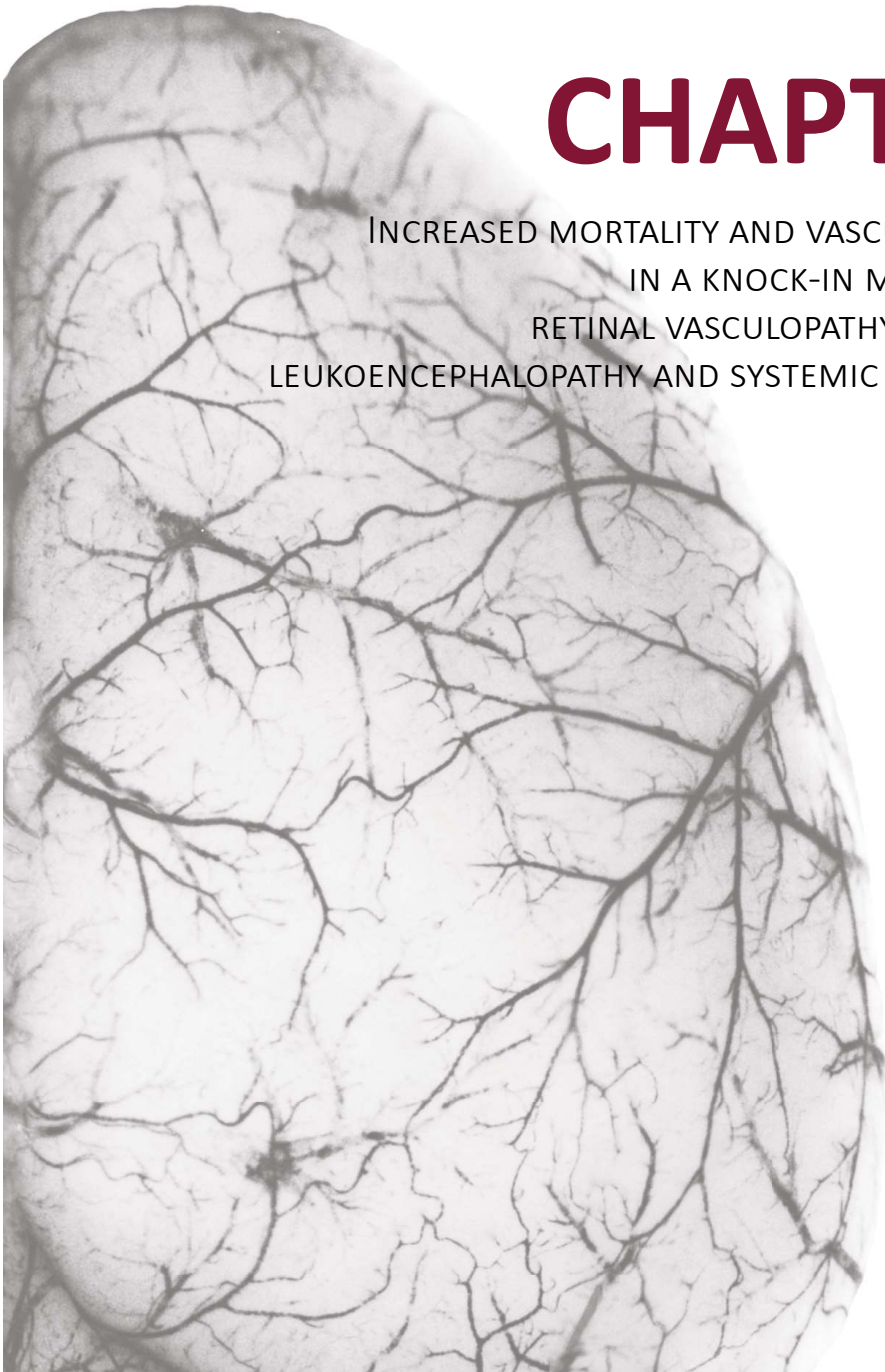Universiteit Leiden

The handle http://hdl.handle.net/1887/138093 holds various files of this Leiden University dissertation.

Author: Mulder, I.A.
Title: Stroke and migraine: Translational studies into a complex relationship
Issue Date: 2020-11-05

CHAPTER 5

INCREASED MORTALITY AND VASCULAR PHENOTYPE
IN A KNOCK-IN MOUSE MODEL OF
RETINAL VASCULOPATHY WITH CEREBRAL
LEUKOENCEPHALOPATHY AND SYSTEMIC MANIFESTATIONS

Mulder IA, Rubio-Beltran E, Ibrahimi K, Dzyubachyk O, Khmelinskii A, Hoehn M, Terwindt GM, Wermer MJH*, MaassenVanDenBrink A*, and van den Maagdenberg AMJM*

*Authors contributed equally

ABSTRACT

Retinal vasculopathy with cerebral leukoencephalopathy and systemic manifestations (RVCL-S) is an autosomal dominant small vessel disease caused by C-terminal frameshift mutations in the *TREX1* gene that encodes the major mammalian 3' to 5' DNA exonuclease. RVCL-S is characterized by vasculopathy, especially in densely vascularized organs, progressive retinopathy, cerebral microvascular disease, white matter lesions, and migraine, but the underlying mechanisms are unknown.

Homozygous transgenic RVCL-S knock-in mice expressing a truncated Trex1 (three prime repair exonuclease 1) protein (similar to what is seen in patients) and wild-type littermates, of various age groups, were subjected to (1) a survival analysis, (2) in vivo postocclusive reactive hyperemia and ex vivo Mulvany myograph studies to characterize the microvascular and macrovascular reactivity, and (3) experimental stroke after transient middle cerebral artery occlusion with neurological deficit assessment.

The mutant mice show increased mortality starting at midlife (P=0.03 with hazard ratio, 3.14 [95% CI, 1.05–9.39]). The mutants also show a vascular phenotype as evidenced by attenuated postocclusive reactive hyperemia responses (across all age groups; $F[1, 65]=5.7$, P=0.02) and lower acetylcholine-induced relaxations in aortae (in 20- to 24-month-old mice; RVCL-S knock-in: E_{max}: 37 ± 8% *vs* WT: E_{max}: 65 ± 6%, P=0.01). A vascular phenotype is also suggested by the increased infarct volume seen in 12- to 14-month-old mutant mice at 24 hours after infarct onset (RVCL-S knock-in: 75.4 ± 2.7 mm^3 *vs* WT: 52.9 ± 5.6 mm^3, P=0.01).

Homozygous RVCL-S knock-in mice show increased mortality, signs of abnormal vascular function, and increased sensitivity to experimental stroke and can be instrumental to investigate the pathology seen in patients with RVCL-S.

5

INTRODUCTION

Retinal vasculopathy with cerebral leukoencephalopathy and systemic manifestations (RVCL-S) is an autosomal dominant disorder caused by C-terminal frameshift mutations in the *TREX1* gene,[1] which encodes the ubiquitously expressed Trex1 (three prime repair exonuclease 1) protein.[1,2] The mechanisms underlying the cause of RVCL-S, however, are unknown. RVCL-S is a systemic progressive small vessel disease with middle-age severe symptomatology and decreased life expectancy, characterized by vasculopathy in various organs, most pronounced in retina, kidney, and brain, with white matter lesions and intracerebral mass lesions.[3-6] Patients with RVCL-S report more often migraine (generally without aura) and have increased risk for ischemic stroke, both suggesting vascular involvement. Pathological studies revealed thicker endothelial cells with increased vesicles and coarse cytoplasm, and thicker, multi-laminated, basement membranes of endothelial cells.[5] Hence it has been hypothesized that the endothelium of small vessels, particularly in highly vascularized organs, is affected in RVCL-S. Endothelial dysfunction (impaired endothelium-dependent vasodilation and endothelial cell damage),[7] which has been proposed as disease mechanism for the vascular phenotype seen in stroke and migraine, was also shown to underlie RVCL-S in patients.[4]

Although patients with RVCL-S are heterozygous for the *TREX1* mutation, here we investigated transgenic homozygous RVCL-S knock-in (KI) mutant mice that express a truncated Trex1 protein (similar to what is seen in patients with RVCL-S).[1,5] The mutant mice express a truncated mouse protein (with the endogenous regulation of gene expression still intact), which is slightly different from the existing humanized RVCL-S mouse model in which the human cDNA bearing the same V235fs mutation was introduced in exon 2 of *TREX1*.[8] Here we assessed whether homozygous RVCL-S KI mice have pathological features seen in patients with RVCL-S, such as a reduced life expectancy and a vascular phenotype (as assessed by functional vascular measurements and induction of experimental stroke).

MATERIALS AND METHODS

The data that support the findings of this study are available from the corresponding author on reasonable request.

Experimental animals

Homozygous transgenic RVCL-S KI and wild-type (WT) littermate mice of different age groups (3–6, 12–14, and 20–24 months) were used. As the heterozygous mutants show a normal survival (Figure 1), we focused on a comparison between the homozygous mutant and WT mice. For the generation of the mutant mice, a targeting construct was used by which a frameshift mutation was introduced at amino acid position 235 of the Trex1 protein, resulting in a truncated protein as observed with the most prevalent RVCL-S mutation in patients (Methods and Supplemental Figure 1).[1,5] Homozygous mutant and WT mice were generated by interbreeding heterozygous mice. For the stroke experiments, only male mice were used. For the in vivo and in vitro vascular characterization, results of both sexes were pooled because no sex difference was detected. Animals were randomized (flip of a coin) for surgical procedure, and researchers were blinded for genotype during experimental and analyses procedures. Animals were housed in a temperature-controlled environment with food and water ad libitum. All animal experiments were approved by the local committee for animal health, ethics and research of the Leiden University Medical Center.

Survival Analysis

Survival in naive WT and homozygous RVCL-S KI mice was assessed in animals who, at 2 months, were randomly assigned to one of the age groups (3–6, 12–14, and 20–24 months) to be included in the experimental stroke studies (n=97). Mice were censored for analysis when they reached the age of inclusion for the stroke experiment. In addition, data of 51 heterozygous animals, which were not used in experiments, were added to the survival analysis.

***In vivo* microvascular characterization**

Microvascular characteristics were assessed in vivo using postocclusive reactive hyperemia (PORH) measurements of the hind leg with laser Doppler flowmetry (PeriFlux System 5000, Perimed, Järfälla-Stockholm, Sweden). Twenty-four hours before dermal blood flow measurements, the hair of the left hind leg was removed with hair removal cream (Veet, ReckittBenckiser, Inc, Berkshire, United Kingdom). On the day of measurement, mice were anesthetized using 4% isoflurane/O_2 ventilation and kept on a heating pad regulated by a rectal thermometer (FHC, Inc, Bowdoin, ME) to maintain body temperature at 36.7 ± 0.3°C. After a 5-minute equilibration time period, 10 minutes of baseline perfusion was recorded. Subsequently, the hind leg circulation was occluded for 2 minutes with a tourniquet. After release of the tourniquet, blood flow was monitored until return to baseline blood flow (maximally 10 minutes). The area under the curve and PORH peak were used as readout measures. After the experimental procedure, mice were euthanized using decapitation, where the aorta was collected for in vitro measurements.

Transient middle cerebral artery occlusion model

Mice were anesthetized using isoflurane (3% induction, 1.5% maintenance) in 70% pressurized air and 30% O_2. Carprofen 5 mg/kg, *s.c.* (Carporal, 50 mg/mL; AST Farma B.V., Oudewater, the Netherlands) was administered before surgery for pain relief. During surgery, the mouse body temperature was maintained at 36.7±0.3°C as described above. Experimental stroke was induced using the transient middle cerebral artery occlusion (MCAO) model.[10] A silicone-coated nylon monofilament (7017PK5Re; Doccol cooperation, Sharon, MA) was introduced into the internal carotid artery, via an incision in the common carotid artery, to block the middle cerebral artery (MCA) at its origin for 30 minutes. Cerebral blood flow in the MCA territory was measured using laser Doppler flowmetry (PeriFlux System 5000; Perimed) and calculated as %-measure of baseline. In a subset of animals, $tcCO_2$ was measured (TCM4 CombiM monitor with accompanying software version 3.0; Radiometer Medical ApS, Brønshøj, Denmark) to confirm physiological stability during surgery (data not shown). After surgery, the animal was placed in a temperature-controlled recovery incubator (V1200; Peco Services Ltd, Brough, United Kingdom) maintained at 33°C for 2 hours, with easy access to food and water. Postprocedural observation was performed twice daily.

Magnetic resonance imaging

Animals were scanned using a small animal 7T MRI system (Pharmascan, Bruker BioSpin, Ettlingen, Germany) under isoflurane anesthesia. A Multi Slice Multi Echo sequence protocol was run with repetition time/echo time of 4.000 ms/9 ms, 20 echoes, 2 averages, matrix 128×128, field of view of 2.50 cm, bandwidth 59523.8 Hz, slice thickness of 0.5 mm, and 16 slices (no gap). Quantitative T2 maps were calculated using Paravision 5.1 software (Bruker

BioSpin). Scans were performed at 4, 24, and 48 hours after MCAO surgery. An in-house developed automated software pipeline[11] was used to calculate infarct sizes. If automated segmentation showed artifacts, for example, due to wrapping, small manual corrections were made, or scans were excluded due to technical failure.

Behavior analyses

Behavior analyses were performed directly before magnetic resonance imaging measurements, that is, before and after (at 4, 24, 48 hours, and 5 days) MCAO surgery. During behavioral tests, mice were videotaped, and blinded videos were analyzed after completion of the experiments. Neurological deficit scores were measured on a 56-point scale.[12,13] The score involved general and focal deficits, where 0 reflected no deficits, and 56 reflected the poorest. Categories concerning general appearance and performance included fur (0–2), ears (0–2), eyes (0–4), posture (0–4), spontaneous activity (0–4), and epileptic behavior (0–12). Concerning the focal deficits a score was stated for body asymmetry (0–4), gait (0–4), climbing on a surface inclined at 45° (0–4), circling behavior (0–4), front-limb symmetry (0–4), compulsory circling (0–4), and whisker response to light touch (0–4).

Vessel anatomy

A subset of mice was used for vessel anatomy analysis.[14,15] In brief, mice were euthanized using CO_2 and transcardially perfused using 2.5 mL PBS with 50 μL heparin (Heparine natrium 5000 I.U./mL; LEO Pharma B.V., Amsterdam, the Netherlands) and 2.5 mL ink mixture (ratio 1:9, Herlitz stempelfarbe ink and Pelikan Scribtol ink; Pelikan Vertriebsgesellschaft mbH & Co. KG, Hannover, Germany) at a rate of 3 mL/min, preheated to 37°C. Brains were removed, photographed, and post-fixated in fresh 4% paraformaldehyde. Vessel anatomy was scored as the number of anastomoses between MCA and anterior cerebral artery, distance between midline, and the anastomotic line at 2, 4, and 6 mm from anterior and diameter of the main vessels of the circle of Willis (MCA, anterior cerebral artery, internal carotid artery, posterior cerebral artery, basilar artery, and posterior communicating artery). Pial anastomoses were defined as the narrowest part of the vessel or halfway between the nearest branch points of the anterior and the MCA, localized by tracing the peripheral branches of these major vessels.

Statistical analyses

All statistical analyses were performed in SPSS software (SPSS statistics 23, IBM Corporation, Armonk, NY). Survival analyses were performed using the log-rank (Mantel-Cox) test, and Cox univariable regression analyses were done to calculate the hazard ratio. Animals who reached the inclusion age of the experiment were censored in the analyses. The PORH results were expressed as relative values compared with baseline and included the area under the curve (AUC) and the maximal hyperemia response (E_{max}), expressed as mean ± SEM. Vascular relaxant responses to acetylcholine and SNP were expressed as the percentage of contraction induced by 10 to 100 nmol/L U46619. Data for the vascular responses to 5-hydroxytryptamine were expressed as percentage of the contractile response to 100 mmol/L KCl. Both the *in vivo* and *in vitro* data were analyzed using univariate ANOVA followed by Bonferroni post hoc tests. Outcome values were expressed as mean ± SEM. Infarct volume and neurological deficit scores were compared between genotypes using marginal mixed model analyses (data are shown as estimated marginal means ± SD). Survival analyses post-surgery were performed using the log-rank (Mantel-Cox) test. Group comparison concerning vessel diameter and anastomotic

distance were analyzed using multivariate ANOVA with discriminant function analysis post hoc test. Absence of the posterior communicating artery was analyzed using Pearson χ2 (2-sided Fisher exact) test, and mean pial number of anastomoses were analyzed with a t test. P < 0.05 indicates statistical significance.

RESULTS

Increased mortality in RVCL-S KI mice

Homozygous RVCL-S KI mutant mice showed increased mortality compared with WT controls: 16 (31%) mutant versus 4 (9%) WT mice died during the observation period presurgery (P=0.03 with hazard ratio, 3.14 [95% CI, 1.05–9.39]). The increased mortality in the mutant mice compared to WT mice was apparent from 9 months of age (Figure 1). Heterozygous mutant mice did not show a reduced lifespan (P=0.55 with hazard ratio, 1.25 [95% CI, 0.60–2.59]; Figure 1). Therefore, only homozygous mutants were investigated in subsequent functional experiments. *Post mortem* examination, although suboptimal because considerable organ deterioration had occurred at the time of tissue examination, did not reveal a macroscopic cause of death (data not shown). *Post mortem* examination also did not show signs of brain atrophy, neither in the heterozygous nor the homozygous mutants, but also here the analysis was not reliable due to organ deterioration (data not shown). Finally, basic histological hematoxylin and eosin staining analyses of various organs (*e.g.*, eye, kidney, skin, liver, brain) of the homozygous and heterozygous mutant mice did not reveal any obvious abnormalities (data not shown). In contrast with patients with RVCL-S,[5] we observed no structural abnormalities in endothelial cells or the basement membrane of the mutant mice. It remains unclear whether this is because these disease features are not captured in the mouse model or whether these features need longer time to develop than the 2-year maximal age of a mouse.
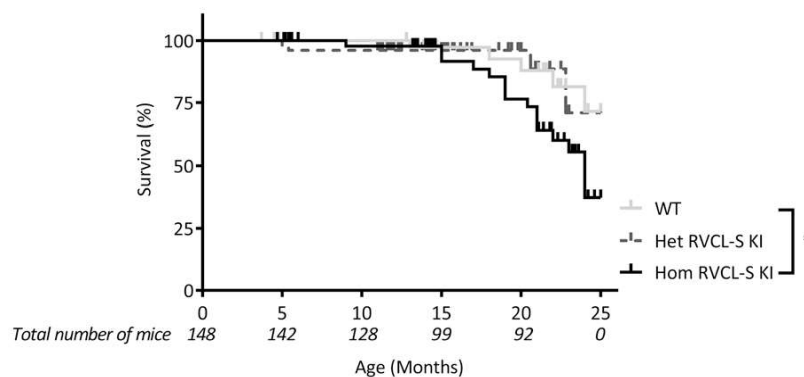
5

Figure 1. Survival curves from wild-type (WT), heterozygous (Het), and homozygous (Hom) retinal vasculopathy with cerebral leukoencephalopathy and systemic manifestations (RVCL-S) knock-in (KI) male mice. At 2 mo, Hom mutant and WT mice were randomly assigned to one of the 3 age groups for experimental stroke surgery. Mice reaching the age of surgical inclusion were censored from the analysis. WT (n=45, gray line), Het RVCL-S KI (n=51, black dotted line), and Hom RVCL-S KI mice (n=52, black line). Vertical bars along curves represent censored animals. WT and Het survival curves were not significantly different. *P<0.05 indicates statistical significance between WT and Hom RVCL-S KI mice.

Reduced *in vivo* microvascular reactivity in RVCL-S KI mice

Compared with WT, the RVCL-S KI mice showed a significantly lower area under the reactive hyperemia curve across all age groups (F[1, 60]=5.1, P=0.03; Figure 2A). The maximal reactive hyperemia responses, however, were comparable between genotypes (Figure 2B). Baseline dermal blood flow and time to maximum value were also similar between genotypes (data not shown).

Increased *in vitro* macrovascular reactivity in RVCL-S KI mice

No significantly different contraction reaction to 100 mmol/L KCl was seen between both genotypes. Instead, the concentration-response curve to acetylcholine showed statistically significantly attenuated relaxant responses in 20- to 24-month-old RVCL-S KI mice compared with WT mice (E_{max}: 65 ± 6% versus 37 ± 8%, respectively, P=0.01), but not in mice of other age groups (Figure 2C). No genotypic difference was observed in the response to SNP or 5-hydroxytryptamine (Figure 2C).

Increased Susceptibility to Experimental Stroke With Worse Outcome in RVCL-S KI Mice.

Overall, infarct volume was higher in RVCL-S KI compared with WT mice (P=0.02), with a significant effect of age (P=0.02) and time after surgery (P<0.001). The effects were mainly driven by the increased infarct volume in RVCL-S KI mice at the age of 12 to 14 months (at 4 hours: RVCL-S KI: 60.4±5.4 *vs* WT: 39.8±4.8 mm³, P=0.007; 24 hours: RVCL-S KI: 84.3±9.5 *vs* WT: 52.9±7.8 mm³, P=0.01; 48 hours: RVCL-S KI: 114.0±13.3 *vs* WT: 58.1±10.7 mm³, P=0.03; Figure
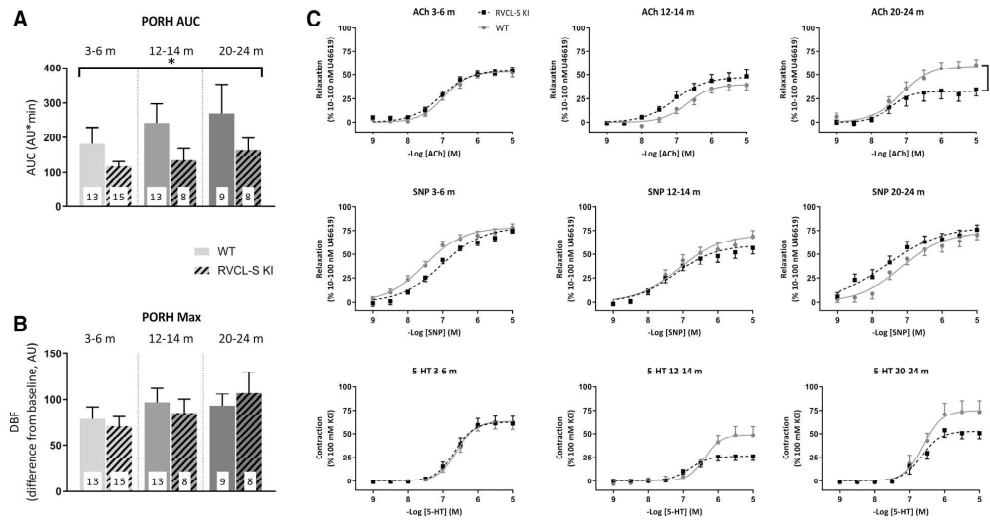

Figure 2. Microvascular and macrovascular characterization of wild-type (WT) and homozygous retinal vasculopathy with cerebral leukoencephalopathy and systemic manifestations (RVCL-S) knock-in (KI) mice. In vivo microvascular characterization using postocclusive reactive hyperemia (PORH) measurements of the hind leg with the area under the reactive hyperemia curve (A) and maximal reactive hyperemia (B) responses for WT and RVCL-S KI mice of the 3 age groups (3–6, 12–14, and 20–24 mo). *p<0.05 indicates a statistical significant difference between RVCL-S KI and WT mice across all age groups. Number of animals is indicated within each bar. (C) In vitro macrovascular characterization of isolated aortae obtained from WT (gray circles) and homozygous RVCL-S KI (black squares) mice. Panels depict concentration-response curves to acetylcholine (ACh, n=7–16), sodium nitroprusside (SNP, n=7–17), and serotonin (5-hydroxytryptamine [5-HT], n=5–15). *p<0.05 indicates statistical significance for attenuated relaxant responses to ACh in 20- to 24-mo-old RVCL-S KI mice compared with WT mice. AU indicates arbitrary units; AUC, area under the curve; DBF, dermal blood flow; M, molar; m, months; and Max, maximal.

3). There was no significant genotypic difference in cerebral vessel anatomy (Supplemental Figure 2 and Table 1). The overall neurological deficit score was worse in RVCL-S KI mice compared to WT for all age groups (P=0.002; Figure 4A). This effect was mainly driven by the 12- to 14-month-old group. In that age group neurological deficit scores was worse in RVCL-S KI than WT after surgery for an extended period of time (at 4 hours: RVCL-S KI: 29.3±3.4 *vs* WT: 11.1±2.9, P<0.001; 24 hours: RVCL-S KI: 24.9±3.4 *vs* WT: 9.9±2.7, P=0.001; 48 hours: RVCL-S KI: 28.5±3.8 *vs* WT: 10.0±2.6, P<0.001; 5 days: 24.2±3.7 *vs* 7.5±2.4, P=0.001), whereas there was no difference before surgery (presurgery: RVCL-S KI: 0.6±0.4 *vs* WT: 0.5±0.2, P=0.20). Mortality within 5 days after stroke onset was also increased in the 12- to 14-month-old group (RVCL-S KI: 7 [8%] *vs* WT: 4 [25%], P=0.04), an effect also present in the 20- to 24-month-old group (RVCL-S KI: 8 [57%] *vs* WT: 2 [13%], P=0.02); the young age group only showed a non-significant trend (RVCL-S KI: 4 [57%] *vs* WT: 2 [33%]). There were no differences in basic parameters such as body weight (Supplemental Table 2) or activity levels (determined from presurgery analyses; Figure 4) between mutant and WT mice that could explain the difference in age-related survival.

DISCUSSION

Here, we investigated whether RVCL-S KI mice, which express a truncated mouse Trex1 protein that mimics the truncated protein seen in patients with the RVCL-S V235fs mutation,[1,5] exhibit features in line with the phenotype of patients with RVCL-S. We demonstrated that homozygous RVCL-S KI mice have (1) a shorter life expectancy, (2) a vascular phenotype, as evidenced by abnormal PORH (microvascular characterization; *in vivo* in hind leg) and
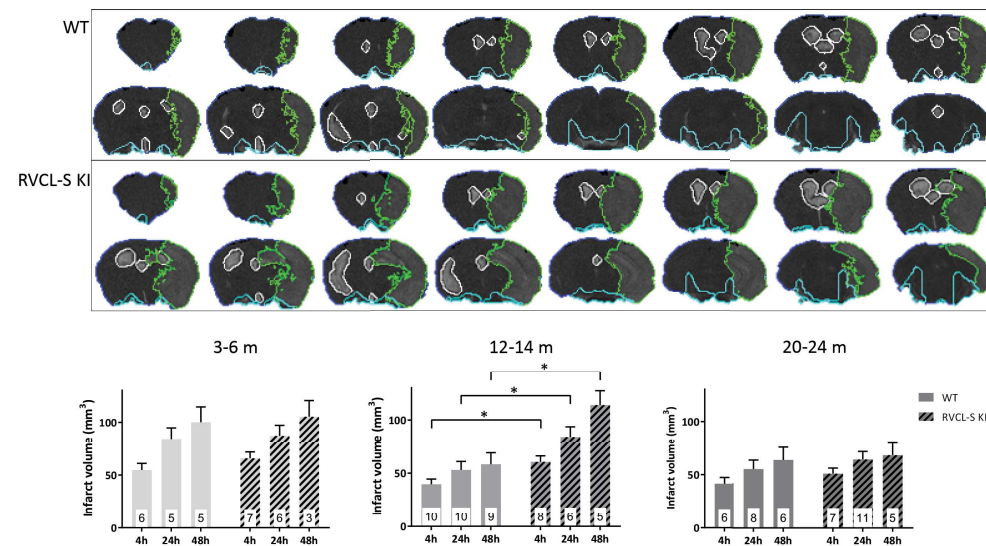

Figure 3. Infarct volume in wild-type (WT) and homozygous retinal vasculopathy with cerebral leukoencephalopathy and systemic manifestations (RVCL-S) knock-in (KI) male mice. A) Example traces of automated stroke segmentation (Green) in T2-weighted magnetic resonance imaging (MRI) images at 24 h after infarct induction in 12- to 14-month-old WT and RVCL-S KI mice. B) Stroke volumes at 4, 24 and 48 h after infarct induction in WT and RVCL-S KI mice of the 3 age groups (3–6, 12–14, and 20–24m; estimated marginal mean ± SD), *p<0.05 indicates a statistically significant difference between 12- to 14-mo-old RVCL-S KI and WT mice for each individual time point. Number of animals is indicated within each bar. Numbers can vary due to death of the animal or technical failure of the MRI scan. h indicates hours; and m indicates months.

acetylcholine-induced relaxant (macrovascular characterization; in vitro in aortic segments) responses, and (3) an increased susceptibility to experimental stroke with a worsened outcome. Except for outcome measures of experimental stroke, the other features can be considered spontaneous phenotypes. Except for signs of abnormal microvascular responses that were already observed from a young age (3–6 months), all other abnormalities were only observed in old mice, that is, in mice of 12 to 14 months and 20 to 24 months. Our study in mice is relevant because it is not understood how vasculopathy, at middle-age, is brought about in patients with RVCL-S and how it is related to the lower life expectancy and increased risk for ischemic stroke.[3–6] Similar to earlier observations in patients with RVCL-S, our data point to decreased functional endothelial responses in mice. In patients, this is exemplified by reduced flow-mediated dilatation responses,[4] and in mice by reduced blood flow after PORH across all investigated ages and by reduced macrovascular relaxant responses to the endothelium-dependent vasodilator acetylcholine.

RVCL-S KI mice have a vascular phenotype

This study is the first to show a vascular phenotype in RVCL-S KI mice. The results of the *in vivo* PORH experiments point towards a microvascular dysfunction, with a decreased AUC of the PORH but a normal maximal PORH peak. As the effect was seen in all age groups, it shows that a vascular phenotype is developing already before the mortality and increased stroke susceptibility become apparent. The PORH response[16] represents an interplay between multiple vasodilation pathways, such as the endothelium-derived hyperpolarizing factor pathway[17] (which is characterized by the AUC) and the release of neuropeptides from perivascular nerves during the hyperemia peak (which is characterized by the maximal hyperemia response [E_{max}]).[18] Notably, in vitro examinations of macrovasculature showed abnormal endothelial function in response to acetylcholine but only in very old RVCL-S KI mice. The decreased relaxant response to acetylcholine seems because of diminished
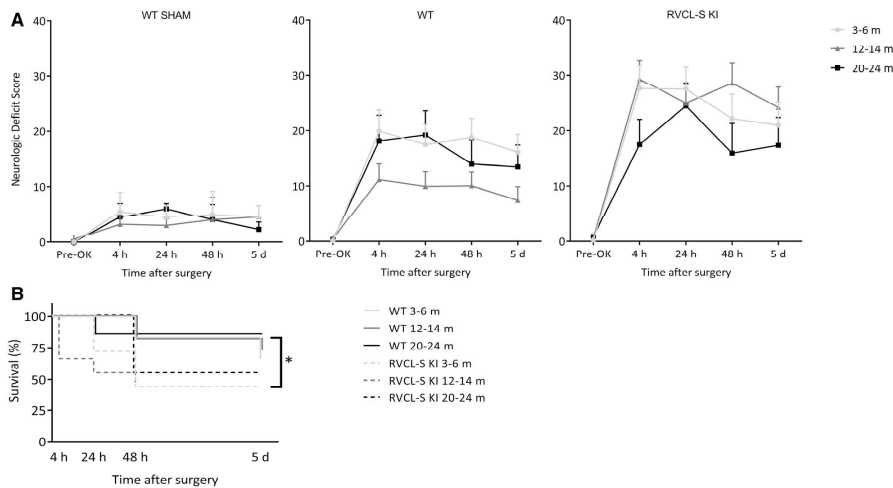

Figure 4. Behavior analysis after infarct induction in wild-type (WT) and homozygous retinal vasculopathy with cerebral leukoencephalopathy and systemic manifestations (RVCL-S) knock-in (KI) male mice. (A) Neurological deficit score (NDS; estimated marginal mean ±SD) for WT SHAM surgery and WT and RVCL-S KI post–transient middle cerebral artery occlusion (MCAO) and (B) survival curves at 4, 24, 48 h and 5 days after MCAO or SHAM surgery in WT (continuous line) and RVCL-S KI mice (discontinuous line) of the 3 age groups (3–6, 12–14, and 20–24 mo). *p<0.05 indicates a statistically significant difference (A) between 12- to 14-mo-old RVCL-S KI and WT mice for NDS and (B) between RVCL-S KI and WT mice concerning survival post-surgery. d indicates days; h, hours; and m, months.

endothelial function, as responses to the endothelium-independent NO donor SNP were normal in RVCL-S KI mice of the same age category. As mentioned above, the in vivo PORH AUC data suggest involvement of an affected endothelium-derived hyperpolarizing factor pathway response. Endothelium-derived hyperpolarizing factor acts as vasorelaxant and is known to act in microvessels rather than in larger vessels.[19,20] Thus, the results of our *in vitro* macrovascular studies are not in contrast with the microvascular PORH results. Testing the natural ligand 5-hydroxytryptamine[21] showed no abnormal vasoconstrictive response in RVCL-S KI mice, although concentration-response curves tended to be lower in the 12- to 14- and 20- to 24-month-old groups compared with WT mice.

Increased Ischemic Vulnerability in RVCL-S KI Mice

The vascular dysfunction seen in RVCL-KI mice may be the underlying cause of increased stroke risk in patients with RVCL-S. Therefore, we investigated whether RVCL-S KI mice had a worse stroke outcome. Although the infarct area is still evolving days to weeks after MCAO, we used 48 hours as final magnetic resonance imaging readout point since infarct size on T2-weighted magnetic resonance imaging is maximized at 48 hours post-MCAO.[22] An overall increased infarct volume was observed in RVCL-S KI mice, compared with WT, albeit driven by the 12- to 14-month-old group. Given the decreased survival in the very old mutant mice, one can envisage that no genotypic difference in infarct volume was seen in the 20- to 24-month-old group because mutant mice that are most affected had already died before reaching the age of inclusion. Endothelial dysfunction was shown to lead to a pro-coagulatory, pro-inflammatory and pro-liferative state, which predisposes to atherosclerosis and increases stroke risk,[7] but it remains to be researched whether this mechanism explains the increased infarct size in RVCL-S KI mice. In future experiments, this should be investigated using electron microscopy for in-depth morphological examination to uncover the possible presence of subtle lesions of the brain endothelium. There remains the, in our view unlikely, possibility that thrombus formation in the vessel after MCAO may have influenced infarct outcome, as we have no *a priori* reason to assume that thrombus formation would be different between mutant and WT mice; although this, admittedly, has not been demonstrated, which would require the use of different methodology than used in the present study.

There are other striking differences for the various age groups when considering infarct size and outcome. Not finding a genotypic effect in young mice may be a reflection that the pathology has not advanced enough, although in vivo microvascular reactivity was already abnormal at that age. As alternative explanation, a genotypic effect may be masked by the seemingly unusually large stroke volume in the respective WT mice, as volumes in WT mice from that age analyzed in our lab usually are 5% to 20% smaller (previously published data[11]). It is even more surprising that mutant mice of 20-24 months have a worse outcome after MCAO but no increased infarct size. One plausible explanation may be inclusion bias. Because animals with large infarcts have a higher *a priori* chance of dying within 48 hours from infarct induction, mice that do survive tend to have smaller infarcts. Apparently, the mutant mice that could be included still exhibit mutation-associated pathology, as reflected by the increased mortality. Such underlying pathology may also explain why a total of 50% of the 20- to 24-month-old RVCL-S KI mice (compared with 15% of the WT group; Figure 1) had already died before scheduled surgery. Of relevance, WT aged male mice (and rats) have smaller infarct volumes,[23] but worse functional outcome,[24,25] when compared with young animals. It remains enigmatic why aged male mice have a decreased infarct size.[26,27] Aged vessels may have undergone morphological and pathological changes,[28] such as structural alterations in

the vessel wall, atherosclerosis and vessel wall calcification,[29,30] small vessel disease,[31] and a reduced impairment of poststroke synaptic plasticity.[27,32]

RVCL-S phenotype in mice *versus* humans

Although the truncated protein product in our KI mouse is very similar to the human canonical *TREX1* frameshift product, one always needs to be cautious when extrapolating data from transgenic mouse models to human disease. Although RVCL-S in humans is an autosomal dominant disorder, the presence of 1 mutated allele causes disease; in our experiments, we focused on homozygotes mice instead to increase chances of capturing disease aspects by doubling the genetic load. It is not uncommon to focus investigations on homozygous mutant mice first as the lifespan in mice (maximal ~2 years) is much shorter than in humans, so a mutation has less time to exert its effect.

In humans, RCVL-S is characterized by various structural abnormalities, foremost the vasculopathy of the retina and other organs, microinfarcts, and white matter lesions.[5,6] A basic histological analysis of the eye and other organs in our mutant mice did not reveal such abnormalities, even not in mice that were far older than 12 months. This can be regarded as a shortcoming of our model, but this disease feature may not be captured because of the shorter lifespan of a mouse. Not finding histological abnormalities in our mutant mice is in accordance with findings in a previously described RVCL-S mouse model,[8,33] that also expresses V235fs-truncated, albeit human, Trex1 protein. In that model, DNase activity, a hallmark of Trex1, was maintained in truncated protein.[33] Both heterozygous and homozygous mutants were reported to be grossly normal with no signs of tissue inflammation; the mutant mice did exhibit striking elevations of auto-antibodies against non-nuclear antigens in the serum.[33] Of note, the authors did not report the decreased survival phenotype, likely because they did not investigate very old mice. We would consider both RVCL-S mouse models equally relevant and having multiple transgenic models will allow replication in separate models.

RVCL-S is considered a small vessel disease.[5] Abnormal functionality of the microvasculature, exemplified by the abnormal PORH response, was observed in mutant mice already of young age. Moreover, in the stroke experiments, outcome (as in human ischemic stroke) is influenced by the status of the microvasculature bed. Both types of experiments show that abnormal functionality of the microvasculature is captured in our mouse model. We recently found that functional endothelial responses were decreased in patients with RVCL-S, while microvascular responses to capsaicin were normal (analyzed using flow-mediated vasodilatation).[4] This points to endothelial dysfunction in RVCL-S, which is in line with our microvascular and macrovascular observations in the homozygous mutant mice. Although flow-mediated vasodilatation responses are generally considered as a measure for macrovascular function, it should be kept in mind that flow-mediated vasodilatation is a physiological response to the increased shear stress during reactive hyperemia and is thus critically dependent on the reactivity of the downstream microvasculature to transient ischemia.

Limitations

As discussed above, our study has several limitations. First, we used homozygous RVCL-S KI mice, although RVCL-S in humans is caused by the presence of only 1 mutated allele, and therefore, translation of the results should be done with caution. Second, several pathological features seen in RVCL-S in humans (ie, vasculopathy of the retina and other organs, microinfarcts, and white matter lesions) were not seen during basic examination

in our model. In future experiments, a more in-depth analysis, for example, using electron microscopy, should be done to address this point. Furthermore, because of study design, we used surviving older animals, which probably have a less severe aging and disease phenotype. It remains an enigma why experimental stroke outcomes in the oldest animals are less severe. In conclusion, we found that the homozygous RVCL-S KI mice exhibit early mortality in line with the reduced life expectancy seen in (heterozygous) patients with RVCL-S. Moreover, we observed a blunted (cerebral) microvascular response suggestive of endothelial involvement, which seems to occur already in young mutant mice, as well as an abnormal macrovascular response in old mutants. Finally, we observed an increased infarct size and worse outcome in homozygous RVCL-S KI mice in response to experimentally induced stroke, but it is at present unclear how this relates to the phenotype in patients with RVCL-S. Regardless, our RVCL-S KI mouse model seems very promising to help unravel the pathophysiology of RVCL-S.

5

REFERENCES

1.   Richards, A, van den Maagdenberg, AM, Jen, JC, Kavanagh, D, Bertram, P, Spitzer, D, *et al.* C-terminal truncations in human 3'-5' DNA exonuclease TREX1 cause autosomal dominant retinal vasculopathy with cerebral leukodystrophy. *Nat Genet.* 2007;39:1068–1070

2.   Mazur, DJ, Perrino, FW. Structure and expression of the TREX1 and TREX2 3' –> 5' exonuclease genes. *J Biol Chem.* 2001;276:14718–14727

3.   Pelzer, N, Bijkerk, R, Reinders, MEJ, van Zonneveld, AJ, Ferrari, MD, van den Maagdenberg, AMJM, *et al.* Circulating endothelial markers in retinal vasculopathy with cerebral leukoencephalopathy and systemic manifestations. *Stroke.* 2017;48:3301–3307

4.   de Boer, I, Stam, AH, Buntinx, L, Zielman, R, van der Steen, I, van den Maagdenberg, AMJM, *et al.* RVCL-S and CADASIL display distinct impaired vascular function. *Neurology.* 2018;91:e956–e963

5.   Stam, AH, Kothari, PH, Shaikh, A, Gschwendter, A, Jen, JC, Hodgkinson, S, *et al.* Retinal vasculopathy with cerebral leukoencephalopathy and systemic manifestations. *Brain.* 2016;139:2909–2922

6.   Terwindt, GM, Haan, J, Ophoff, RA, Groenen, SM, Storimans, CW, Lanser, JB, *et al.* Clinical and genetic analysis of a large Dutch family with autosomal dominant vascular retinopathy, migraine and Raynaud's phenomenon. *Brain.* 1998;121(pt 2):303–316

7.   Lee, S, Kim, W, Park, J, Jang, HH, Lee, SM, Woo, JS, *et al.* Effects of electroacupuncture on endothelial function and circulating endothelial progenitor cells in patients with cerebral infarction. *Clin Exp Pharmacol Physiol.* 2015;42:822–827

8.   Hasan, M, Fermaintt, CS, Gao, N, Sakai, T, Miyazaki, T, Jiang, S, *et al.* Cytosolic nuclease TREX1 regulates oligosaccharyltransferase activity independent of nuclease activity to suppress immune activation. *Immunity.* 2015;43:463–474

9.   Chan, KY, Edvinsson, L, Eftekhari, S, Kimblad, PO, Kane, SA, Lynch, J, *et al.* Characterization of the calcitonin gene-related peptide receptor antagonist telcagepant (MK-0974) in human isolated coronary arteries. *J Pharmacol Exp Ther.* 2010;334:746–752

10.   Longa, EZ, Weinstein, PR, Carlson, S, Cummins, R. Reversible middle cerebral artery occlusion without craniectomy in rats. *Stroke.* 1989;20:84–91

11.   Mulder, IA, Khmelinskii, A, Dzyubachyk, O, de Jong, S, Rieff, N, Wermer, MJ, *et al.* Automated ischemic lesion segmentation in MRI mouse brain data after transient middle cerebral artery occlusion. *Front Neuroinform.* 2017;11:3

12.   De Simoni, MG, Storini, C, Barba, M, Catapano, L, Arabia, AM, Rossi, E, *et al.* Neuroprotection by complement (C1) inhibitor in mouse transient brain ischemia. *J Cereb Blood Flow Metab.* 2003;23:232–239

13.   Storini, C, Rossi, E, Marrella, V, Distaso, M, Veerhuis, R, Vergani, C, *et al.* C1-inhibitor protects against brain ischemia-reperfusion injury via inhibition of cell recruitment and inflammation. *Neurobiol Dis.* 2005;19:10–17

14.   Eikermann-Haerter, K, Lee, JH, Yuzawa, I, Liu, CH, Zhou, Z, Shin, HK, *et al.* Migraine mutations increase stroke vulnerability by facilitating ischemic depolarizations. *Circulation.* 2012;125:335–345

15.   Hasan, MR, Herz, J, Hermann, DM, Doeppner, TR. Intravascular perfusion of carbon black ink allows reliable visualization of cerebral vessels. *J Vis Exp.* 2013;4:4374

16.   Ibrahimi, K, De Graaf, Y, Draijer, R, Danser, AH, Maassen VanDenBrink, A, van den Meiracker, AH. Reproducibility and agreement of different non-invasive methods of endothelial function assessment. *Microvasc Res.* 2018;117:50–56

17.   Cracowski, JL, Gaillard-Bigot, F, Cracowski, C, Sors, C, Roustit, M, Millet, C. Involvement of cytochrome epoxygenase metabolites in cutaneous postocclusive hyperemia in humans. *J Appl Physiol.* (1985). 2013;114:245–251

18.   Larkin, SW, Williams, TJ. Evidence for sensory nerve involvement in cutaneous reactive hyperemia in humans. *Circ Res.* 1993;73:147–154

19.   Danser, AH, Tom, B, de Vries, R, Saxena, PR. L-NAME-resistant bradykinin-induced relaxation in porcine coronary arteries is NO-dependent: effect of ACE inhibition. *Br J Pharmacol.* 2000;131:195–202

20.   Hwa, JJ, Ghibaudi, L, Williams, P, Chatterjee, M. Comparison of acetylcholine-dependent relaxation in large and small arteries of rat mesenteric vascular bed. *Am J Physiol.* 1994;266:H952–H958

21.   Gupta, S, Mehrotra, S, Villalón, C, De Vries, R, Garrelds, I, Saxena, P, *et al.* Effects of female sex hormones on responses to CGRP, acetylcholine, and 5-HT in rat isolated arteries. *Headache.* 2007;47:564–575

22.   Neumann-Haefelin, T, Kastrup, A, de Crespigny, A, Yenari, MA, Ringer, T, Sun, GH, *et al.* Serial MRI after transient focal cerebral ischemia in rats: dynamics of tissue injury, blood-brain barrier damage, and edema formation. *Stroke.* 2000;31:1965–72; discussion 1972

23.   Liu, F, Yuan, R, Benashski, SE, McCullough, LD. Changes in experimental stroke outcome across the life span. *J Cereb Blood Flow Metab.* 2009;29:792–802

24.   Badan, I, Buchhold, B, Hamm, A, Gratz, M, Walker, LC, Platt, D, *et al.* Accelerated glial reactivity to stroke in aged rats correlates with reduced functional recovery. *J Cereb Blood Flow Metab.* 2003;23:845–854

25.   Popa-Wagner, A, Badan, I, Walker, L, Groppa, S, Patrana, N, Kessler, C. Accelerated infarct development, cytogenesis and apoptosis following transient cerebral ischemia in aged rats. *Acta Neuropathol.* 2007;113:277–293

26.   Wang, RY, Wang, PS, Yang, YR. Effect of age in rats following middle cerebral artery occlusion. *Gerontology.* 2003;49:27–32

27.   Sieber, MW, Claus, RA, Witte, OW, Frahm, C. Attenuated inflammatory response in aged mice brains following stroke. *PLoS One.* 2011;6:e26288

28.   Manwani, B, Friedler, B, Verma, R, Venna, VR, McCullough, LD, Liu, F. Perfusion of ischemic brain in young and aged animals: a laser speckle flowmetry study. *Stroke.* 2014;45:571–578

29.   Lakatta, EG. Arterial and cardiac aging: major shareholders in cardiovascular disease enterprises: Part III: cellular and molecular clues to heart and arterial aging. *Circulation.* 2003;107:490–497

30.   Herrera, MD, Mingorance, C, Rodríguez-Rodríguez, R, Alvarez de Sotomayor, M. Endothelial dysfunction and aging: an update. *Ageing Res Rev.* 2010;9:142–152

31.   Popa-Wagner, A, Pirici, D, Petcu, EB, Mogoanta, L, Buga, AM, Rosen, CL, *et al.* Pathophysiology of the vascular wall and its relevance for cerebrovascular disorders in aged rodents. *Curr Neurovasc Res.* 2010;7:251–267

32.   Sieber, MW, Guenther, M, Jaenisch, N, Albrecht-Eckardt, D, Kohl, M, Witte, OW, *et al.* Age-specific transcriptional response to stroke. *Neurobiol Aging.* 2014;35:1744–1754

33.   Sakai, T, Miyazaki, T, Shin, DM, Kim, YS, Qi, CF, Fariss, R, *et al.* DNase-active TREX1 frame-shift mutants induce serologic autoimmunity in mice. *J Autoimmun.* 2017;81:13–23

SUPPLEMENTAL MATERIAL

METHODS

Generation and characterization of transgenic *TREX1* V235fs knock-in mice.

The mouse *TREX1* gene was modified using a gene targeting approach, in such a manner that the gene product was truncated at amino acid position 235 (which is a Threonine codon in the mouse gene and a Valine codon in the human gene) and contained the same abnormal amino acid sequence until the new stop codon as seen in RVCL-S patients with the V235fs mutation (for details on the sequences, see Supplemental Figure 1D).

Targeting construct for the generation of RVCL-S KI mice (Supplemental Figure 1A).
The targeting construct contained the RVCL-S mutation and a PGK-driven neomycin selection cassette (Neo), flanked by LoxP sites, which had been introduced downstream of *TREX1* and upstream of neighbouring Scotin, between the polyA (pA) sequences of both genes.

Targeting ES cells and confirmation of correctly targeted alleles in mice by Southern blot analysis (Supplemental Figure 1B).
E14 ES cells were targeted according to standard procedures, and selected, correctly targeted, ES cells were injected into C57BL/6J blastocysts. Obtained chimeras were bred with C57BL/6J mice and germline transmission of the mutant allele was obtained, thus creating mice with the "RVCL-S + Neo" allele. The selection cassette was then removed by crossing the mutant mice with mice of the EIIA-Cre deleter strain[1] (in which Cre recombinase expression is driven by the EIIA early promoter), which resulted in mice with the RVCL-S KI allele. Heterozygous RVCL-S KI mice were subsequently interbred to provide mice with homozygous mutant and wildtype genotypes. Confirmation of correct targeting was obtained by Southern blotting of EcoRI-digested genomic DNA (from cortex) of mice of the various genotypes (*i.e.* before and after Cre-mediated recombination). Upstream (5') and downstream (3') probes (as depicted in Supplemental Figure 1A) were used for Southern blotting.

Verification of truncated Trex1 protein by Western blot analysis (Supplemental Figure 1C).
Expression of truncated Trex1 protein was confirmed by semi-quantitative Western blotting. To this end, cortex tissue of wildtype and homozygous RVCL-S KI mice that had been killed by cervical dislocation was used. Whole cell lysates were homogenized with a potter (ice-cooled), followed by short sonication using RIPA-buffer in the presence of protease inhibitor cocktail (Cat. No. 1836 170, Roche, Mannheim, Germany). Concentrations were measured (Pierce BCA Protein Assay Kit (Thermo, Cat#23225)) and 2 µg was loaded on a 15% PAA gel. After separation, proteins were transferred onto a nitrocellulose membrane. Blots were blocked with PBS/5% low fat milk/0.05% Tween-20 and subsequently incubated for 2 hours at room temperature with primary anti-mouse Trex1 antibody (BD transduction material number 611986). (1:2,500 diluted in incubation buffer (PBS/0.05% Tween-20). Secondary peroxidase labelled Rabbit anti-mouse antibody (DAKO, P0260) (1:2,000 diluted in incubation buffer) incubation was performed for 1 hour at room temperature. Primary actin antibody incubation was performed for 2 hours at room temperature (A2066, Sigma, St Louis, MO, USA) (1:2,000 diluted in incubation buffer). Secondary peroxidase-labelled Swine anti-rabbit antibody (DAKO, P0217) (1:2,000 diluted in incubation buffer) incubation was performed for 1 hour at room temperature. Western blotting was done according to the enhanced chemiluminescence ECL

protocols (Amersham). Semi-quantification was based on equal β-actin signal intensity (loading control) and revealed Trex1 protein bands of 26 KDa for the mutant allele (as predicted from the truncation) and 33 KDa for the wildtype gene product.

Direct Sanger sequencing of RT-PCR products verified expression of V235fs mutation containing RNA (Supplemental Figure 1D).

The presence of the truncation mutation at the RNA level was confirmed by direct sequence analysis of RT-PCR product. To this end, RNA was extracted from cortex of wildtype and homozygous RVCL-S KI mice that had been killed by cervical dislocation. Total RNA was isolated using RNA Instapure (Eurogentec, Seraing, Belgium). For RT-PCR, first-strand cDNA was synthesized using random primers, and subsequent PCR was performed using Trex1-specific primers (primer sequences are available from the authors upon request). PCR products were sequenced using standard conditions.

Details on the nature of human and mouse wildtype and mutant *TREX1/TREX1* sequences are provided for comparison. In brief, the relevant part of wildtype mouse *TREX1* sequence starting with the Valine codon at position 235, followed by a sequence of Thr-Ala-Ser-Ala, was changed to a sequence of His-Ser-Leu-Cys, followed by the premature stop codon, in the mutant sequence.

REFERENCES

1   Lakso M, Pichel JG, Gorman JR, Sauer B, Okamoto Y, Lee E, et al. Efficient in vivo manipulation of mouse genomic sequences at the zygote stage. Proc Natl Acad Sci USA. 1996;93:5860-5865.

FIGURES
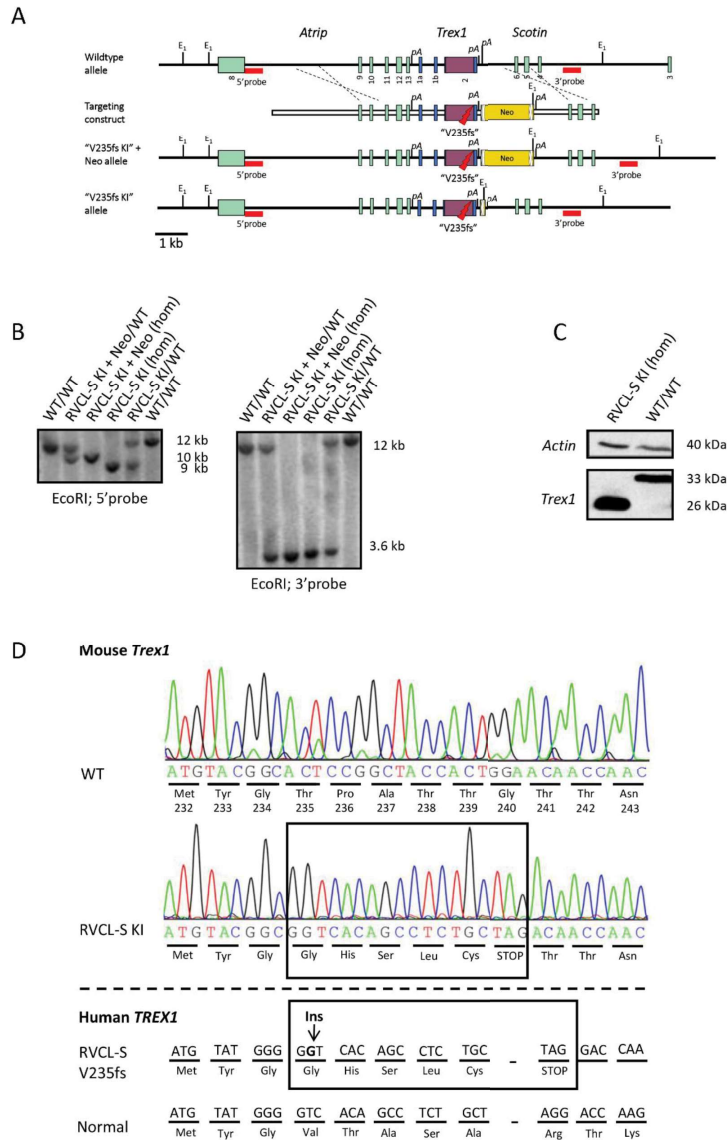
Supplemental Figure 1. Generation and molecular characterization of RVCL-S KI mice. (A) The relevant part of the genomic structure of the wildtype *TREX1* allele, the targeting vector, and the predicted gene structure after homologous recombination ("V235fs KI + Neo" allele), and after Cre-mediated deletion of the Neo-cassette (Neo) (depicted as a yellow box) ("V235fs KI" allele) are shown. Numbered boxes indicate exons of *Atrip, Scotin* and *TREX1* genes. The position of the "V235fs" mutation in *TREX1*'s coding exon 2 (purple box) is indicated. Red horizontal lines indicate probes for Southern blot analysis. EcoRI restriction sites are marked as E1, polyadenylation signal sites are marked as pA. B) Southern blots of EcoRI-digested genomic DNA obtained from mice with the indicated combinations of the RVCL-S KI + Neo, RVCL-S KI, and wildtype alleles. Respective bands obtained with either the 5'- or the 3'-probe are indicated. WT: wildtype; Hom: homozygote. C) Western blot of cortex protein lysate isolated from wildtype (WT/WT) and homozygous (hom) RVCL-S KI mice probed with Trex1 or actin antibody reveals expression of truncated (26 KDa) or normal-sized (33 KDa) Trex1 protein; note that higher levels of Trex1 protein are present in the mutant compared to wildtype mice. D) Electropherograms of relevant parts (black boxes) of *TREX1* obtained from direct sequencing of RT-PCR products of cortex. Total RNA isolated from wildtype (WT) and homozygous RVCL-S KI mice are shown. For comparison, the respective sequences of mutant (RVCL-S) and normal human *TREX1* are shown below the dotted horizontal line.

107
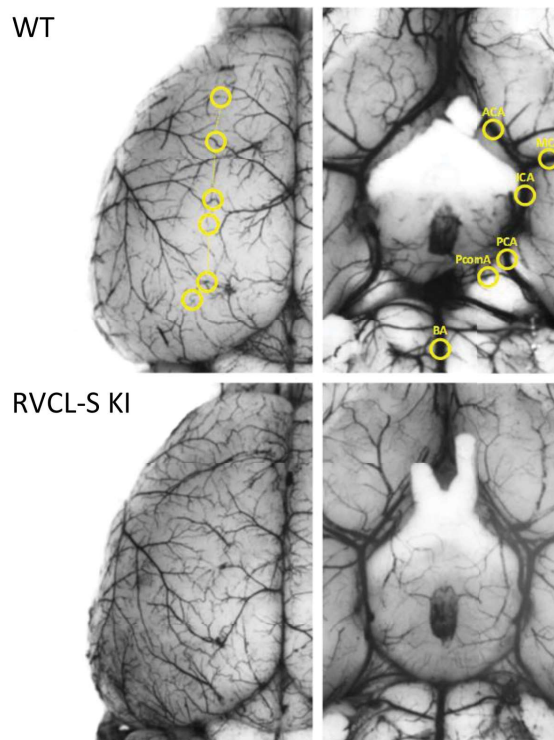
Supplemental Figure 2. Representative examples of cerebral main vessel anatomy analysis of the Circle of Willis and pial collaterals in wildtype (WT) and homozygous RVCL-S KI mice. Representative ventral and dorsal views of WT and RVCL-S KI brains show the circle of Willis anatomy and pial arterial anastomoses between middle and anterior cerebral arteries. Pictures were taken after transcardiac ink perfusion under deep isoflurane anesthesia. Circles on the dorsal surface indicate examples of analyzed pial anastomoses (number and distance to midline were analyzed), whereas circles on the ventral surface indicate measurement areas for arterial diameters. None of these endpoints significantly differed between WT and RVCL-S KI mice (Supplemental Table 1).

TABLES

	WT (n=8)	RVCL-S KI (n=9)	p
ACA diameter (μm)	116 ± 26	114 ± 18	0.849
BA diameter (μm)	182 ± 24	168 ± 19	0.203
ICA diameter (μm)	150 ± 23	138 ± 16	0.101
MCA diameter (μm)	123 ± 24	111 ± 14	0.254
PCA diameter (μm)	132 ± 21	119 ± 15	0.080
PcomA diameter (μm)	31 ± 15	29 ± 10	0.559
# mice with unilaterally absent PcomA (n)	2	3	1.000
# pial anastomoses between MCA and ACA (n)	7.3 ± 1.21	7.6 ± 0.88	0.686
Anastomoses distance from midline (mm)			
Rostral 1/3 of cortex	1.76 ± 0.26	1.66 ± 0.16	0.335
Middle 1/3 of cortex	1.82 ± 0.31	1.70 ± 0.13	0.263
Caudal 1/3 of cortex	1.95 ± 0.29	1.95 ± 0.21	0.978

Supplemental Table 1. Cerebrovascular anatomy obtained using transcardiac ink perfusion. The representative images and the method of measurements can be found in Supplemental Figure II. ICA – Internal Carotid Artery; MCA – Middle Cerebral Artery; ACA – Anterior Cerebral Artery; PCA – Posterior Cerebral Artery; BA – Basilar Artery; PcomA – Posterior communicating Artery.

5

Weight before surgery (mean (g) ± SD)	3–6 months (n=13)	12–14 months (n=28)	20–24 months (n=31)
WT	33.6 ± 2.0	39.6 ± 4.8	36.5 ± 4.5
RVCL-S KI	32.3 ± 3.2	38.0 ±3.0	35.6 ± 5.3

Supplemental Table 2. Animal weight (Mean ± SD) per genotype and age group, measured the day of the surgical procedure (MCAO or SHAM surgery). SD – Standard deviation.